Life Sciences 234 (2019) 116777

Contents lists available at ScienceDirect

Life Sciences

journal homepage: www.elsevier.com/locate/lifescie

Plasma membrane proteins: A new probe for the characterization of breast cancer

Heba M. Fahmy[a,*], Alaa M. Ismail[a], Amena S. El-Feky[a], Esraa S. Abu Serea[b], Wael M. Elshemey[a,c]

[a] Biophysics Department, Faculty of Science, Cairo University, 12613 Giza, Egypt
[b] Chemistry and Biochemistry Department, Faculty of Science, Cairo University, 12613 Giza, Egypt
[c] Department of Physics, Faculty of Science, Islamic University in Madinah, kSA

ARTICLE INFO

Keywords:
FTIR
Breast cancer
Plasma membrane proteins
Benign
Malignant

ABSTRACT

This work aimed to characterize normal, benign and malignant excised breast tissues through the analysis of the FTIR spectra of their plasma membrane proteins. Tissue characterization parameters such as peak position, peak intensity, area under the peak, relative peak intensity and relative area under peak were evaluated mainly for protein spectral peaks; 1150 cm^{-1}, Amide *I*, Amide II, Amide III, and Amide A. The sensitivity, specificity and diagnostic accuracy for each parameter were obtained and Receiver Operating Characteristic (ROC) Curves were plotted. Results showed significant spectral differences between normal and benign tissues compared to malignant tissues at 1536 and 1645 cm^{-1}. The three tissues could be distinguished at 2900 cm^{-1}, where the malignant peak uniquely split into two separate peaks. ROC curves showed that the Amide A peak position yielded a higher accuracy compared to all other investigated characterization parameters. The deconvolution of Amide I revealed the conformational changes in plasma proteins characterizing the transformation to malignancy (a decrease in the percentage of alpha helix accompanied by an increase in the percentage of beta sheets). The use of the present structure-based analysis in conjunction with histopathological examination of excised breast tissues would offer an enhanced characterization that might reduce possible personal diagnostic mistakes.

1. Introduction

Breast cancer is the most common cancer and the main cause of cancer-related death in women [1,2]. It is reported that its incidence is still increasing [3,4]. In 2018, about 627,000 women died due to breast cancer, representing about 15% of all cancer deaths among women [5]. The annual number of new breast cancer cases per 100,000, varies globally as 27 in Middle Africa and Eastern Asia, 89 in Western Europe and 92 in Northern America [6].

Massive efforts have been exerted in order to offer a reliable mean for the diagnosis of breast cancer. This includes the differentiation between benign and malignant tumors using a wide range of proposed methods and techniques [7–12].

Following diagnosis with breast cancer, mastectomy is one of the main treatments of choice [13–15]. After mastectomy, it is crucially important to provide accurate histopathological characterization of the excised breast tumor, mainly, for being benign or malignant. This would define the following medical course. An incorrect diagnosis may lead to life-threatening consequences. A variety of tools have been proposed for the characterization of excised breast tissues. These tools would help in avoiding possible personal diagnostic mistakes in addition to inter- and intra-observer variability [16–22].

Vibrational spectroscopic procedures, including FTIR spectroscopy, are probable techniques for non-invasive optical tissue diagnosis. Currently, the use of spectroscopic techniques in biological investigations has expanded a lot. Clinical examinations related to cancer diagnosis using spectroscopic tools have attracted the attention of clinical and non-clinical researchers [23–27].

Infrared spectroscopy is one of the oldest and well-established experimental techniques for the analysis of the secondary structure of polypeptides and proteins [28–30]. It has been used in the characterization of a wide-range of compounds and biomolecules [31–33]. Fourier Transform Infra-red (FTIR) has been applied to the characterization of several cancer types [34–38].

FTIR spectroscopy has been extensively used for the characterization of benign and malignant excised breast tissues using different approaches and analytical procedures [39–43].

FTIR investigations of breast tissues have been carried out mainly on the whole tissue without further extractions [41,43]. Although this holds the advantage of time saving and simplicity, yet it makes the

* Corresponding author.
E-mail address: hfahmy@sci.cu.edu.eg (H.M. Fahmy).

https://doi.org/10.1016/j.lfs.2019.116777
Received 2 July 2019; Received in revised form 8 August 2019; Accepted 15 August 2019
Available online 26 August 2019

obtained results molecularly nonspecific. In other words, it cannot be related to changes, for example, in certain protein or group of proteins.

The aim of this work is to investigate the ability of characterizing normal, benign and malignant excised breast tissues via extensive analysis of the FTIR spectra of their plasma membrane proteins. The study involves the introduction and evaluation of tissue characterization parameters in terms of sensitivity, specificity and diagnostic accuracy obtained from the cutoff values of scatter diagrams. Data are further analysed using Receiver Operating Characteristic (ROC) Curves in addition to the deconvolution of Amide I plasma protein peak. This offers a unique secondary structure-based characterization of different breast tissues.

2. Materials and methods

2.1. Sample preparation

Excised breast tissue specimens were collected over a period of one month for women undergoing mastectomy. These samples were taken just before sample disposal. The samples are completely obscure and cannot be linked to specific patients. A histopathologist classified the specimens into 15 normal, 15 malignant, and 15 benign tissues. The total number of tissues investigated in the present study was chosen according to previous related studies [44,45].

The samples were maintained at -80°C until further use. Ab65400 Kit (Abcam, United States) was used to extract plasma membrane proteins from excised breast tissue samples. This kit provides optimized buffers and reagents for efficient extraction of membrane proteins from mammalian tissues. According to the kit manufacturer, this kit offers a consistent yield and high purity (over 90%). The same kit has been used by too many authors for the same purpose in their recently published work [47–49].

2.2. Fourier transform infrared (FTIR) spectroscopy

FTIR spectroscopy was carried out for the extracted plasma membrane proteins from all breast tissue samples. Tissues are ground with KBr in the ratio of 1:100 and compressed using a hydraulic press under a pressure of 15,000 lbs. The pellets were scanned in an inert atmosphere over a wave number range of 4000–400 cm^{-1} using Hitachi 295 spectrophotometer (Jasco, Mod 4100, Japan). The control (normal), benign and malignant tissues were all subject to the same treatment, therefore, the observed spectral changes will be probably related to corresponding changes in the different samples.

2.3. Data processing

The FTIR spectra of normal, benign, and malignant samples were acquired, area normalized and the average spectrum of each of the three tissue categories was calculated. Five absorption peaks; at 1150 cm^{-1} (C-O-C stretching mode of carbohydrates), 1240 cm^{-1} (Amide III mode), 1536 cm^{-1} (due to N—H bending coupled to a C—N stretching vibrations), 1645 cm^{-1} (due to C═O stretching vibration) and 3456 cm^{-1} (due to N—H stretching) were used to investigate the difference between normal, benign, and malignant samples. A set of recommended FTIR characterization parameters (peak position, peak intensity, area under the peak, relative intensity and relative area) were employed, for the five selected peaks, to get quantitative values for the substantive characteristics of different FTIR spectra. The mean area under peak parameter was calculated from the spectral data using the trapezoidal integration method with the help of Microsoft Excel 2010. The relative intensity and relative area under peak parameters were determined by dividing the band area and band intensity of Amide I peak at 1645 cm^{-1} (sensitive to protein secondary structure) by the band area and band intensity of each of the remaining 1150, 1240, 1536 and 3456 cm^{-1} peaks.

Duncan multiple range test was carried out utilizing the IBM SPSS 17 statistical software package to evaluate whether the selected spectral peaks could significantly differentiate between the three tissue types using the suggested five characterization parameters, which were seen as a possible diagnostic test for the characterization of each breast tissue type and malignant lesions.

2.3.1. Diagnostic indices of scatter diagrams

Scatter diagrams are a tool to calculate the sensitivity, specificity and diagnostic accuracy of diagnostic tests. In this work, they showed each breast tissue type on the x-axis and the corresponding individual values of a certain diagnostic test on the y-axis. The optimum cutoff value was calculated by the Index of Union approach as described in [50], at which the cutoff value taken at a point where the difference between sensitivity and specificity is minimum. The horizontal line represented the cutoff value of malignant samples and was used to differentiate them from normal and benign samples.

The diagnostic sensitivity is the percentage of samples with the disease diagnosed properly by the test as positive (true positive divided by the total of true positive and false negative). The diagnostic specificity is the percentage of samples without the disease specified properly by the test as negative (true negative divided by the total of true negative and false positive). The diagnostic accuracy is the percentage of samples properly particularized as true positive and true negative out of all tested samples (the total of true positive and true negative divided by the total number of samples) [51,52].

2.3.2. Receiver Operating Characteristic (ROC) curves

To evaluate the performance of diagnostic tests, the standard Receiver Operating Characteristic (ROC) curve method was used [17,18]. A ROC curve was obtained by changing the cutoff values above and under the optimum cutoff and evaluating the corresponding specificity and sensitivity [17,53–55]. The evaluation of a desirable diagnostic characterization parameter was determined by calculating the area under the ROC curve (AUC). A value of AUC in the range of 0.5–0.7 indicated a poorly accurate test. A test value of 0.7–0.9 indicated a moderately accurate test, while a highly accurate test had a value of 0.9–1.0. The test was non-informative when AUC was < 0.5, while a perfect test had an AUC value equal to unity [54,56].

2.3.3. Second derivative and deconvolution of Amid I band

A seven-point Savitzky–Golay filter was used to obtain smoothed area-normalized FTIR spectra and their corresponding second derivative spectra were obtained using Origin 8.0 software [17,57–59]. Spectral peak deconvolution was applied to uncover the protein secondary structure components comprising the Amide I band (1600–1700 cm^{-1}) of the investigated breast tissue samples [60,61]. Since this band arises from the C═O stretching vibration of the peptide group and its frequency depends on hydrogen bonding and coupling of the polypeptide backbone, it is sensitive to protein conformation [62]. The spectral deconvolution of Amide I absorption band was achieved via Gaussian curve fitting tool in Origin 8.0 software, where the elements of protein secondary structure were determined using the frequencies predicted by the second derivative [57,63]. The peak positions, widths and heights corresponding to different protein secondary structure components were thus elucidated [64].

3. Results & discussion

3.1. The average spectra of plasma membrane proteins for distinct samples

The average spectra of each of the investigated samples (Fig. 1) reveal a superior absorption of plasma membrane proteins from malignant tissues over those from normal and benign ones. Notably, the malignant spectra demonstrate the highest absorption peaks at amide II (1540–1570 cm^{-1}) and Amide I (1600–1700 cm^{-1}), in line with the

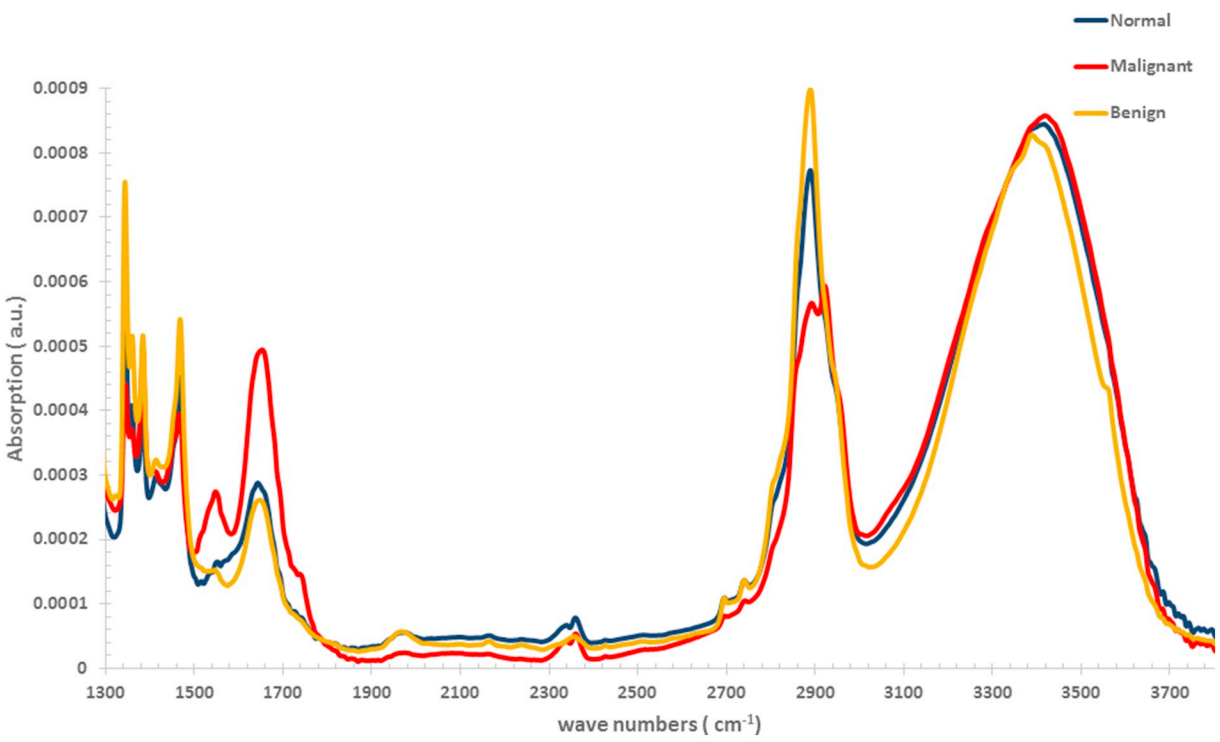

Fig. 1. Average spectra of plasma membrane proteins after area normalization of the spectra of individual samples designated in blue for normal, red for malignant and golden yellow for benign. (For interpretation of the references to colour in this figure legend, the reader is referred to the web version of this article.)

proteomics data in [65,66].

Surprisingly, the absorption peak around 2900 cm^{-1} due to CH_2/CH_3 stretching vibrations [41,67] apparently separates the three candidates. The existence of this peak is attributed to the presence of lapidated peptides in plasma membrane proteins [68,69]. Noteworthy, the malignant sample is the only one that splits into two peaks at 2887 cm^{-1} & 2918 cm^{-1}.

3.2. FTIR-breast tissue characterization

The statistical significance of breast tissue characterization using the parameters driven from the absorption peaks at 1150 cm^{-1}, 1240 cm^{-1}, 1536 cm^{-1}, 1645 cm^{-1} and 3456 cm^{-1} are calculated using Duncan multiple range test. Table 1 introduces the characterization parameters which significantly ($p < 0.05$) distinguish between plasma membrane proteins from different breast tissues, yet, the parameters providing non-significant characterization results are not listed. The parameters significantly distinct normal and benign samples from those of malignant samples (area under peak and peak intensity at 1536 and 1645 cm^{-1}, intensity ratio (1645/3456 cm^{-1}) and area under peak ratios (1645/1150 cm^{-1} and 1645/3456 cm^{-1}). It also shows significant ($p < 0.05$) differentiation between normal and malignant samples using the peak position parameter at 1645 cm^{-1} and between normal and benign samples (at area under peaks 1150 cm^{-1} and 1240 cm^{-1} and peak position 3456 cm^{-1}). Despite most characterization parameters are unable to discriminate between normal and benign samples, yet the later parameters represent a bright spot to rely on as they can significantly distinguish between benign and normal samples. Although, the last two parameters (area under the Amide III peak at 1240 cm^{-1} and peak position shift of Amide A at 3456 cm^{-1}) poorly distinguish plasma membrane proteins from normal and malignant tissues. Therefore, they can be utilized in conjunction with the other successful characterization parameters to characterize the three tissue types using FTIR analysis of their plasma membrane proteins.

3.3. Sensitivity, specificity and ROC curves

Table 2 shows the sensitivity, specificity and diagnostic accuracy of

Table 1
Characterization parameters and bands that are significantly able to distinguish between membrane proteins of the three candidates ($P < 0.05$). Values with different symbols are statistically different according to Duncan's test results.

Characterization parameters		Normal	Benign	Malignant
Area under peak	1150 cm^{-1}	0.027 ± 0.004 ^{a}	0.033 ± 0.005 ^{b}	0.023 ± 0.005 ^{a}
	1240 cm^{-1}	0.011 ± 0.002 ^{a}	0.014 ± 0.001 ^{b}	0.012 ± 0.001 ^{a,b}
	Amide I (1645 cm^{-1})	0.023 ± 0.005 ^{a}	0.020 ± 0.008 ^{a}	0.038 ± 0.018 ^{b}
	Amide II (1536 cm^{-1})	0.008 ± 0.004 ^{a}	0.008 ± 0.003 ^{a}	0.014 ± 0.008 ^{b}
Peak intensity	Amide I (1645 cm^{-1})	0.0003 ± 0.0 ^{a}	0.0002 ± 0.0 ^{a}	0.0005 ± 0.0 ^{b}
	Amide II (1536 cm^{-1})	0.0002 ± 0.0 ^{a}	0.0002 ± 0.0 ^{a}	0.0003 ± 0.0 ^{b}
Peak position	Amide I (1645 cm^{-1})	1644.08 ± 7.714 ^{a}	1645.35 ± 5.388^{a,b}	1649.87 ± 6.286 ^{b}
	Amide A (3456 cm^{-1})	3408.18 ± 14.331 ^{a}	3387.27 ± 14.767 ^{b}	3413.16 ± 13.124^{a}
Intensity ratio	1645/3456 cm^{-1}	0.355 ± 0.095 ^{a}	0.319 ± 0.097 ^{a}	0.593 ± 0.277 ^{b}
Area under peak ratio	1645/1150 cm^{-1}	0.862 ± 0.303 ^{a}	0.651 ± 0.339 ^{a}	1.870 ± 1.315 ^{b}
	1645/1240 cm^{-1}	2.267 ± 1.136 ^{a,b}	1.495 ± 0.724 ^{a}	3.111 ± 1.561 ^{b}
	1645/3456 cm^{-1}	0.076 ± 0.021 ^{a}	0.072 ± 0.023 ^{a}	0.123 ± 0.052 ^{b}

Table 2
Sensitivity, Specificity and Diagnostic accuracy of selected characterization parameters that significantly differentiate malignant from normal and benign samples. Amide A, peak position also differentiates between normal and benign samples.

Characterization parameters		Sensitivity (%)	Specificity (%)	Diagnostic Accuracy (%)
Area under peak	Amide I	69.2	68	70.3
	Amide II	61.5	59.1	60
Peak intensity	Amide I	69.2	75	72.9
	Amide II	69.2	66.7	67.6
Peak position	Amide A to differ between Benign and malignant	84.6	84.6	84.6
	Amide A to differ between Normal and benign	72.7	69.2	70.8

the investigated characterization parameters to differentiate breast tissue samples at the optimal cutoff values. Fig. 2 (a, b) presents the scatter diagrams used for the calculation of the diagnostic indices for intensity and area under Amide I peak (1640 cm^{-1}) parameters for the characterization of malignant from normal and benign samples. The corresponding area under the ROC curves (0.837 and 0.801, respectively) for the two parameters are presented in Fig. 3 (a, b). This confirms the capability of the FTIR technique to differentiate malignant samples from normal and benign ones. The AUC values of the ROC curves of the ratio of intensities and areas at 1645/3400 cm^{-1} (Data not shown) are 0.808 and 0.801, respectively. The intensity and area of the 1536 cm^{-1} peak show AUC values of 0.744 and 0.734, respectively (Data not shown) indicating slightly less accurate performance to set apart malignant from normal and benign samples compared to the other parameters.

The ROC curves in Fig. 3 (c, d), obviously, confirms the extent of characetrication accuracy of Amide A (3400 cm^{-1}) peak position parameter, yielding AUC values of 0.825 and 0.858 that are considered accurate in distinguishing between c) normal and benign and d) benign and malignant samples, respectively.

3.4. Band narrowing technique and protein secondary structure

FTIR is an outstanding technique in its sensitivity to conformational changes in proteins. In this work, protein secondary structure is extensively investigated utilizing a band narrowing technique (the second derivative of the acquired FTIR spectra) and the deconvolution of Amide I peak (1640 cm^{-1}). Fig. 4 illustrates the second derivative spectra of the three breast plasma membrane protein samples in Amide I region (1600–1700 cm^{-1}). One can notice that each spectrum appears fractioned into distinct secondary structure components. Notably the peak at 1650 cm^{-1} appears as two separate minima in the benign spectrum (1648.9 & 1652.7 cm^{-1}) compared to normal while it completely disappears in the malignant one. This attitude refers to the reduction of alpha helix component of malignant proteins [39].

Additionally, the shift to lower wave number 1627 cm^{-1} of benign and malignant spectra at 1630 cm^{-1} (beta strands) compared to normal can ultimately differentiate normal proteins from tumors. This shift refers to the induction of conformational changes in benign and malignant proteins.

Table 3 shows the plasma membrane proteins-secondary structural components of each candidate and its percentage (revealed after deconvolution of the Amide I peak). Interestingly, the shift from normal to malignant state accompanied by a change in secondary structure from helix to sheets, besides a slight increase in the percentage of random coils and aggregates. This clearly interprets the spectral changes in the Amide I region of the second derivative spectra. Up to the authors' knowledge, this is the first time that FTIR spectra of plasma membrane proteins are used as a probe for the detection of breast cancer.

In a previous work by the same authors [41], the FTIR spectra of whole tissues were used to differentiate between the three breast tissues (normal, benign and malignant). The problem with the previous study is that it was not possible to relate the observed changes in the FTIR spectra of different tissues to a specific group of proteins. That is why the present study focuses only on plasma membrane proteins to unveil their possible contribution to the changes in the FTIR spectra of breast tissues. Although the measurements of whole tissues would be much easier, yet, in fact, the measurements of extracted proteins would be much more informative in terms of structural information on the involved proteins.

Changes in peak position originate mainly from conformational differences between plasma membrane proteins in different tissue types. One common conformational change is the transformation from alpha helix to beta sheet conformation. It is difficult in the present stage to correlate these changes to a specific protein. It will need further extensive proteomic analysis.

4. Conclusion

It is shown that extensive analysis of the FTIR spectra of plasma membrane proteins from normal, benign and malignant breast tissue samples can successfully characterize all three tissues. It was interesting to note that the shift from normal to malignant state was accompanied by a change in secondary structure from helix to sheets, besides a slight increase in the percentage of random coils and aggregates. The merit is

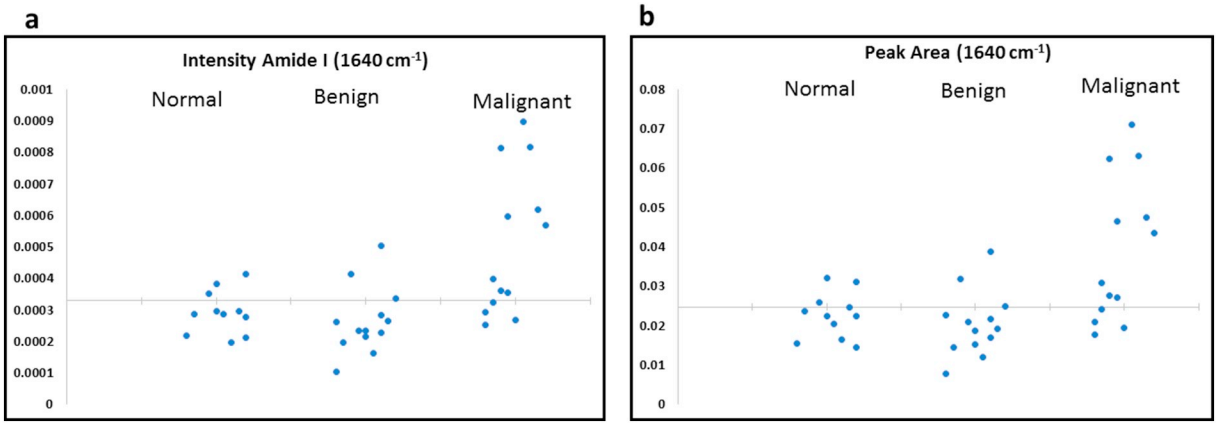

Fig. 2. Scatter diagram for (a) Intensity and (b) area under Amide I band at 1640 cm^{-1}. The horizontal line is the optimal cut-off value to set apart malignant from normal and benign samples.

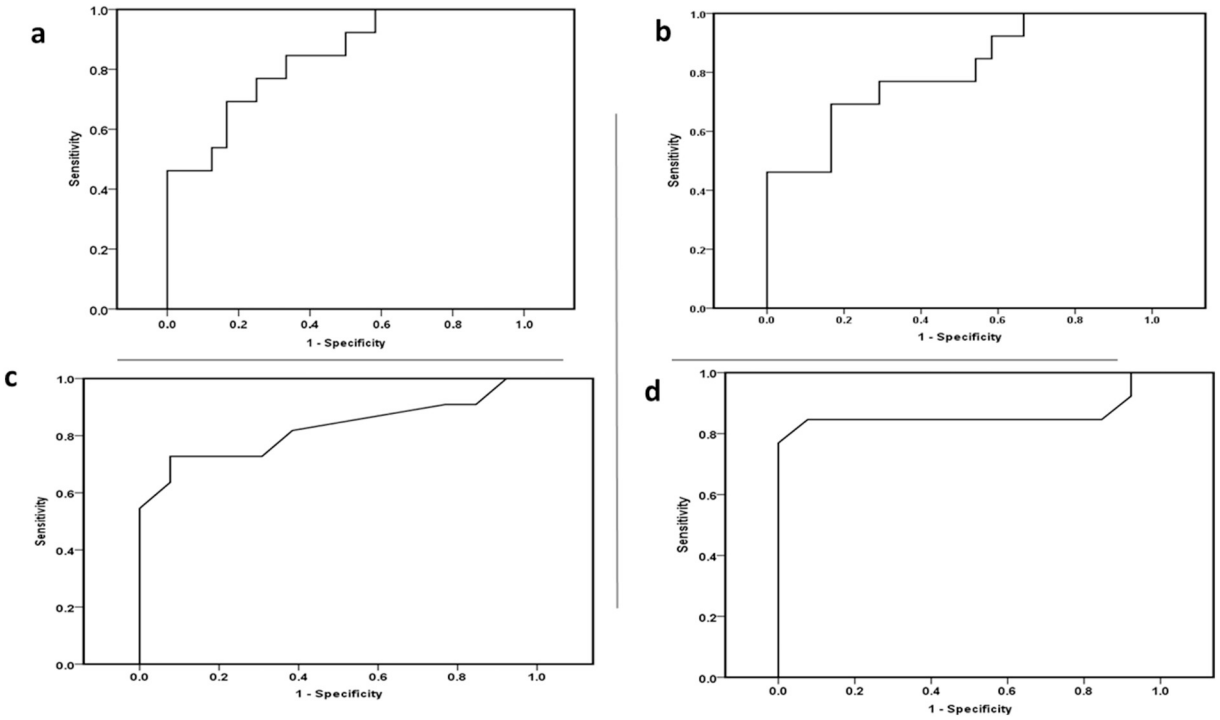

Fig. 3. ROC curves for (a) Intensity and (b) area under Amide I band at 1640 cm^{-1} to set apart malignant from normal and benign samples. Area under ROC curves are 0.837 and 0.801 for a and b, respectively. (c) and (d) ROC curves for Amide A peak position at 3400 cm^{-1} to distinguish between normal and benign and benign and malignant samples, respectively. Area under ROC curves are 0.825 and 0.858 for c and d, respectively.

that, this characterization is based on the protein structural changes accompanying the transformation to malignancy. This is a new perspective that is independent on personal judgement and may help to reduce possible personal errors associated with histopathological diagnosis. We recommend the use of FTIR as a confirmation tool in conjunction with the histopathological analysis/diagnosis of cancerous tissues. Once a contradiction between both results is detected, the histopathological Analysis/Diagnosis should be rechecked by one or more histopathologists.

Acknowledgment

This work is supported by a research project granted from Cairo University, Egypt.

The authors would like to acknowledge the cooperation of Dr. Mohammed S Mohammed, National cancer centre (NCR), Cairo, Egypt.

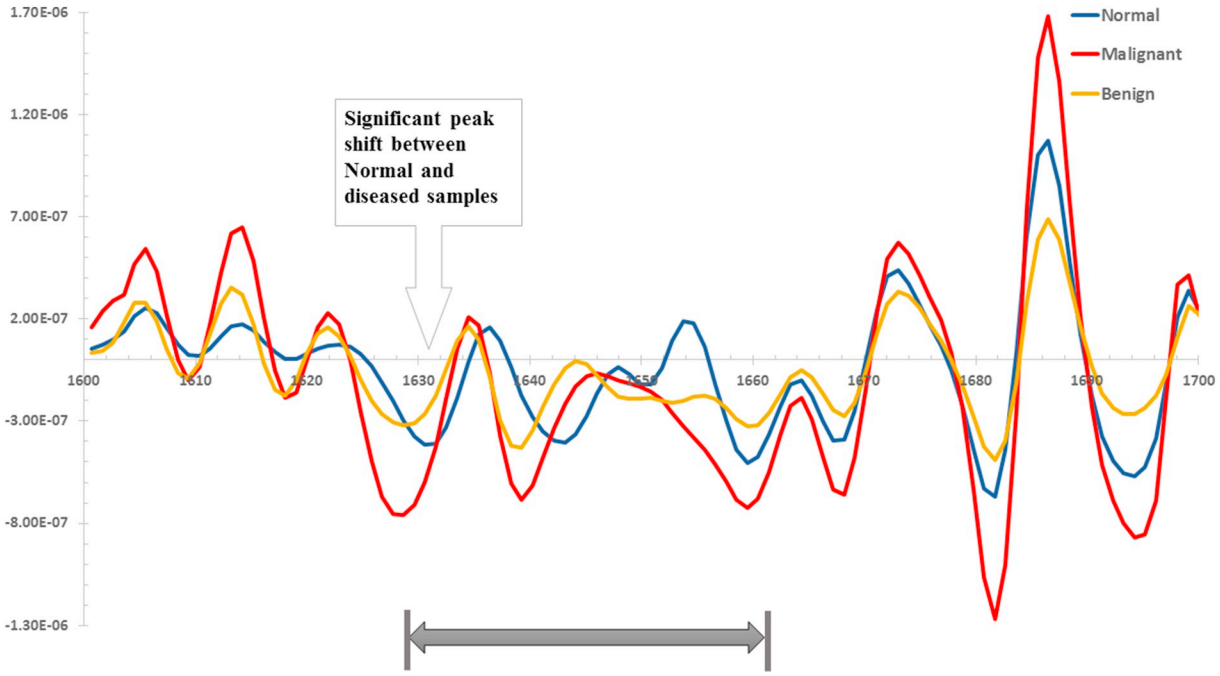

Fig. 4. Second derivative for Amide I band. The bidirectional arrow assigns the region where benign and malignant samples shift from normal.

Table 3
Secondary structure components of membrane proteins for each of normal, benign and malignant samples deconvoluted from the Amide I band. The percentage of each conformational structure is shown. Values with different symbols are statistically different according to Duncan's test results.

Area under deconvolved peak (1600–1700 cm^{-1})	Normal	Benign	Malignant
Alpha helix (1648–1660 cm^{-1})	0.0026 ± 0.003 [a]	0.0015 ± 0.002 [a]	0.0046 ± 0.004 [b]
(1660–1670 cm^{-1})	45.5%	39.8%	31.7%
Beta sheets/turns	0.001 ± 0.0 [a]	0.0011 ± 0.002 [a]	0.0031 ± 0.0 [b]
(1625–1640 cm^{-1})	32.6%	38.2%	44.5%
(1670–1695 cm^{-1})			
Random Coil	0.0009 ± 0.0 [a]	0.001 ± 0.001 [a]	0.0029 ± 0.002 [b]
(1640–1648 cm^{-1})	9%	9.2%	10.1%
Aggregated strands	0.0014 ± 0.0 [a,b]	0.0008 ± 0.001 [a]	0.0025 ± 0.002 [b]
(1610–1628 cm^{-1})	12.9%	12.8%	13.7%

References

[1] A. De, G. Kuppusamy, V.V.S.R. Karri, Affibody molecules for molecular imaging and targeted drug delivery in the management of breast cancer, Int. J. Biol. Macromol. 107 (2018) 906–919.
[2] A. Ghannam, H. Murad, M. Jazzara, A. Odeh, A.W. Allaf, Isolation, structural characterization, and antiproliferative activity of phycocolloids from the red seaweed Laurencia papillosa on MCF-7 human breast cancer cells, Int. J. Biol. Macromol. 108 (2018) 916–926.
[3] R.L. Siegel, K.D. Miller, A. Jemal, Cancer statistics, CA Cancer J. Clin. 66 (1) (2016) 7–30.
[4] N. Qin, S. Lu, N. Chen, C. Chen, Q. Xie, X. Wei, F. Ye, J. He, Y. Li, L. Chen, L. Jiang, Yulangsan polysaccharide inhibits 4T1 breast cancer cell proliferation and induces apoptosis in vitro and in vivo, Int. J. Biol. Macromol. 121 (2019) 971–980.
[5] World Health Organization, Technical Report: Pricing of Cancer Medicines And Its Impacts: A Comprehensive Technical Report for the World Health Assembly Resolution 70.12: Operative Paragraph 2.9 on Pricing Approaches and their Impacts on Availability and Affordability of Medicines for the Prevention and Treatment of Cancer, (2018).
[6] J. Ferlay, I. Soerjomataram, R. Dikshit, S. Eser, C. Mathers, M. Rebelo, D.M. Parkin, D. Forman, F. Bray, Cancer incidence and mortality worldwide: sources, methods and major patterns in GLOBOCAN 2012, Int. J. Cancer 136 (5) (2015) 359–386.
[7] Z. Li, L. Yu, X. Wang, H. Yu, Y. Gao, Y. Ren, G. Wang, X. Zhou, Diagnostic performance of mammographic texture analysis in the differential diagnosis of benign and malignant breast tumors, Clin. Breast Cancer 18 (4) (2018) 621–627.
[8] S. Punitha, A. Amuthan, K.S. Joseph, Benign and malignant breast cancer segmentation using optimized region growing technique, Future Comput. Inform. J. 3 (2) (2018) 348–358.
[9] N. Liu, E.S. Qi, M. Xu, B. Gao, G.Q. Liu, A novel intelligent classification model for breast cancer diagnosis, Inf. Process. Manag. 56 (3) (2019) 609–623.
[10] H. Tan, J. Chen, Y. ling Zhao, J. huan Liu, L. Zhang, C. sheng Liu, D. Huang, Feasibility of intravoxel incoherent motion for differentiating benign and malignant thyroid nodules, Acad. Radiol. 26 (2) (2019) 147–153.
[11] C. Núñez, Blood-based protein biomarkers in breast cancer, Clin. Chim. Acta 490 (2019) 113–127.
[12] D.M. Vo, N.Q. Nguyen, S.W. Lee, Classification of breast cancer histology images using incremental boosting convolution networks, Inf. Sci. 482 (2019) 123–138.
[13] R. Barnawi, S. Al-Khaldi, G. Majed Sleiman, A. Sarkar, A. Al-Dhfyan, F. Al-Mohanna, H. Ghebeh, M. Al-Alwan, Fascin is critical for the maintenance of breast cancer stem cell pool predominantly via the activation of the notch self-renewal pathway, Stem Cells 34 (12) (2016) 2799–2813.
[14] Y. Jiang, J. Li, H. Lin, Q. Huang, T. Wang, S. Zhang, Q. Zhang, Z. Rong, J. Xiong, The efficacy of gabapentin in reducing pain intensity and morphine consumption after breast cancer surgery: a meta-analysis, Medicine 97 (38) (2018).
[15] L. van Manen, J. Eggermont, O. Dzyubachyk, A. Fariña-Sarasqueta, A.L. Vahrmeijer, J.S.D. Mieog, J. Dijkstra, February. Snapshot hyperspectral imaging for detection of breast tumors in resected specimens, Diseases in the Breast and Reproductive System V, 10856 International Society for Optics and Photonics, 2019, p. 108560I.
[16] W.M. Elshemey, W.B. Elsharkawy, Monte Carlo simulation of x-ray scattering for quantitative characterization of breast cancer, Phys. Med. Biol. 54 (12) (2009) 3773.
[17] W.M. Elshemey, O.S. Desouky, M.M. Fekry, S.M. Talaat, A.A. Elsayed, The diagnostic capability of x-ray scattering parameters for the characterization of breast cancer, Med. Phys. 37 (8) (2010) 4257–4265.
[18] W.M. Elshemey, F.S. Mohamed, I.M. Khater, X-ray scattering for the characterization of lyophilized breast tissue samples, Radiat. Phys. Chem. 90 (2013) 67–72.
[19] D.W. Shipp, K. Kong, E. Rakha, I. Ellis, I. Notingher, October. Raman spectral histopathology of breast cancer recession margins, Laser Science, Optical Society of America, 2016, pp. JW4A–112.
[20] A. Chan, J.A. Tuszynski, Automatic prediction of tumour malignancy in breast cancer with fractal dimension, R. Soc. Open Sci. 3 (12) (2016) 160558.
[21] J. Chang, J. Yu, T. Han, H.J. Chang, E. Park, A method for classifying medical images using transfer learning: A pilot study on histopathology of breast cancer, 2017 IEEE 19th International Conference on e-Health Networking, Applications and Services (Healthcom), IEEE, 2017, pp. 1–4.
[22] W. Xie, Y. Chen, Y. Wang, L. Wei, C. Yin, A.K. Glaser, M.E. Fauver, E.J. Seibel, S.M. Dintzis, J.C. Vaughan, N.P. Reder, Microscopy with ultraviolet surface excitation for wide-area pathology of breast surgical margins, J. Biomed. Opt. 24 (2) (2019) 26501.
[23] Z. Movasaghi, S. Rehman, I.U. Rehman, Raman spectroscopy can detect and monitor cancer at cellular level: analysis of resistant and sensitive subtypes of testicular cancer cell lines, Appl. Spectrosc. Rev. 47 (7) (2012) 571–581.
[24] T.C. Bowman, M. El-Shenawee, L.K. Campbell, Terahertz imaging of excised breast tumor tissue on paraffin sections, IEEE Trans. Antennas Propag. 63 (5) (2015) 2088–2097.
[25] G. Thomas, T.Q. Nguyen, I.J. Pence, B. Caldwell, M.E. O'Connor, J. Giltnane, M.E. Sanders, A. Grau, I. Meszoely, M. Hooks, M.C. Kelley, Evaluating feasibility of an automated 3-dimensional scanner using Raman spectroscopy for intraoperative breast margin assessment, Sci. Rep. 7 (1) (2017) 13548.
[26] D.M. McClatchy III, E.J. Rizzo, J. Meganck, J. Kempner, J. Vicory, W.A. Wells, K.D. Paulsen, B.W. Pogue, Calibration and analysis of a multimodal micro-CT and structured light imaging system for the evaluation of excised breast tissue, Phys. Med. Biol. 62 (23) (2017) 8983.
[27] P.E. Summers, A. Vingiani, S. Di Pietro, A. Martellosio, P.F. Espin-Lopez, S. Di Meo, M. Pasian, M. Ghitti, M. Mangiacotti, R. Sacchi, P. Veronesi, Towards mm-wave spectroscopy for dielectric characterization of breast surgical margins, Breast 45 (2019) 64–69.
[28] J. Kong, S. Yu, Fourier transform infrared spectroscopic analysis of protein secondary structures, Acta Biochim. Biophys. Sin. 39 (8) (2007) 549–559.
[29] V. Arumugam, M. Venkatesan, K. Ramachandran, S. Ramachandran, S.K. Palanisamy, U. Sundaresan, Purification, characterization and antibacterial properties of peptide from marine ascidian Didemnum sp, Int. J. Pept. Res. Ther. (2019) 1–8.
[30] W.M. Elshemey, I.A. Mohammad, A.A. Elsayed, Wide-angle X-ray scattering as a probe for insulin denaturation, Int. J. Biol. Macromol. 46 (2010) 471–477.
[31] E.V. Wilson, M.J. Bushiri, V.K. Vaidyan, Characterization and FTIR spectral studies of human urinary stones from Southern India, Spectrochim. Acta A Mol. Biomol. Spectrosc. 77 (2) (2010) 442–445.
[32] N. Igci, P. Sharafi, D.O. Demiralp, C.O. Demiralp, A. Yuce, S.D. Emre, Application of Fourier transform infrared spectroscopy to biomolecular profiling of cultured fibroblast cells from Gaucher disease patients: a preliminary investigation, Adv. Clin. Exp. Med. 26 (7) (2017) 1053–1061.
[33] R. Golabiazar, K.I. Othman, K.M. Khalid, D.H. Maruf, S.M. Aulla, P.A. Yusif, Green synthesis, characterization, and investigation antibacterial activity of silver nanoparticles using Pistacia atlantica leaf extract, BioNanoScience (2019) 1.
[34] D. Max, L. Chiriboga, P. Lasch, A. Pacifico, IR spectra and IR spectral maps of individual normal and cancerous cells, Biopolymers: Original Research on Biomolecules 67 (4–5) (2002) 349–353.
[35] D.E. M., M.T. Do, F.M. Shamji, S.R. Sundaresan, D.G. Perkins, P.T.T. Wong, Fourier-transform infrared spectroscopic study of characteristic molecular structure in cancer cells of esophagus: an exploratory study, Cancer Detect. Prev. 31 (3) (2007) 244–253.
[36] K., Catherine, M. Isabelle, F. Bazant-Hegemark, J. Hutchings, L. Orr, J. Babrah, R. Baker, N. Stone. Vibrational spectroscopy: a clinical tool for cancer diagnostics. Analyst 134, no. 6 (2009) 1029–1045.
[37] B. Giuseppe, C. Sorio, Infrared spectroscopy and microscopy in cancer research and diagnosis, Am. J. Cancer Res. 2 (1) (2012) 1.
[38] L., Cássio, V. Goulart, L. Côrrea, T. Pereira, D. Zezell. ATR-FTIR spectroscopy for the assessment of biochemical changes in skin due to cutaneous squamous cell carcinoma. Int. J. Mol. Sci. 16, no. 4 (2015) 6621–6630.
[39] R. Eckel, H. Huo, H.W. Guan, X. Hu, X. Che, W.D. Huang, Characteristic infrared spectroscopic patterns in the protein bands of human breast cancer tissue, Vib. Spectrosc. 27 (2) (2001) 165–173.
[40] H. Fabian, N.A.N. Thi, M. Eiden, P. Lasch, J. Schmitt, D. Naumann, Diagnosing benign and malignant lesions in breast tissue sections by using IR-microspectroscopy, Biochim. Biophys. Acta Biomembr. 1758 (7) (2006) 874–882.
[41] W.M. Elshemey, A.M. Ismail, N.S. Elbialy, Molecular-level characterization of normal, benign, and malignant breast tissues using FTIR spectroscopy, J. Med. Biol. Eng. 36 (3) (2016) 369–378.
[42] M. Verdonck, A. Denayer, B. Delvaux, S. Garaud, R. De Wind, C. Desmedt, C. Sotiriou, K. Willard-Gallo, E. Goormaghtigh, Characterization of human breast cancer tissues by infrared imaging, Analyst 141 (2) (2016) 606–619.
[43] R. Mehrotra, G. Tyagi, S. Charak, B. Ray, G. Kadayaprath, H. Chaturvedi, U. Mukherjee, A. Abrari, Biospectroscopic analysis of human breast cancer tissue:

probing infrared signatures to comprehend biochemical alterations, J. Biomol. Struct. Dyn. 36 (3) (2018) 761–766.
[44] J. Henrik, F. Socciarelli, N.M. Vacanti, M.H. Haugen, Y. Zhu, I. Siavelis, A. Fernandez-Woodbridge, et al., Breast cancer quantitative proteome and proteogenomic landscape, Nat. Commun. 10 (1) (2019) 1600.
[45] W. Kathrin E., F. Großerueschkamp, H. Jütte, M. Horn, F. Roghmann, N. von Landenberg, T. Bracht et al. Integrated Fourier transform infrared imaging and proteomics for identification of a candidate histochemical biomarker in bladder cancer. Am. J. Pathol. 189, no. 3 (2019) 619–631.
[50] I. Unal, Defining an optimal cut-point value in roc analysis: an alternative approach, Comput. Math. Methods Med. 2017 (2017).
[51] D.A. Grimes, K.F. Schulz, Uses and abuses of screening tests, Lancet 359 (2002) 881–884.
[52] M.E. El-Houseini, M.S. Mohammed, W.M. Elshemey, T.D. Hussein, O.S. Desouky, A.A. Elsayed, Enhanced detection of hepatocellular carcinoma, Cancer Control 12 (4) (2005) 248–253.
[53] R.B.M. Landewe, D.M.F.M. Heijde, Principles of assessment from a clinical perspective, Best Pract. Res. Clin. Rheumatol. 17 (3) (2003) 365–379.
[54] M. Greiner, D. Pfeiffer, R.D. Smith, Principles and practical application of the receiver-operating characteristic analysis for diagnostic tests, Prev. Vet. Med. 45 (2000) 23–41.
[55] J.A. Swets, Measuring the accuracy of diagnostic systems, Science 24 (1988) 1285–1293.
[56] F. Habibzadeh, P. Habibzadeh, M. Yadollahie, On determining the most appropriate test cut-off value: the case of tests with continuous results, Biochemia medica: Biochemia medica 26 (3) (2016) 297–307.
[57] H. Susi, D.M. Byler, Protein structure by Fourier transform infrared spectroscopy: second derivative spectra, Biochem. Biophys. Res. Commun. 115 (1) (1983) 391–397.
[58] L. Jørgensen, C. Vermehren, S. Bjerregaard, S. Froekjaer, Secondary structure alterations in insulin and growth hormone water-in-oil emulsions, Int. J. Pharm. 254 (2003) 7–10.
[59] B. Sarmento, D.C. Ferreira, L. Jorgensen, V.M. Weert, Probing insulin's secondary structure after entrapment into alginate/chitosan nanoparticles, Eur. J. Pharm. Biopharm. 65 (2007) 10–17.
[60] P.I. Haris, F. Severcan, FTIR spectroscopic characterization of protein structure in aqueous and non-aqueous media, J. Mol. Catal. B Enzym. 7 (1999) 207–221.
[61] L.M. Miller, M.W. Bourassa, R.J. Smith, FTIR spectroscopic imaging of protein aggregation in living cells, Biochim. Biophys. Acta Biomembr. 1828 (2013) 2339–2346.
[62] A. Barth, Infrared spectroscopy of proteins, Biochim. Biophys. Acta Biomembr. 1767 (2007) 1073–1101.
[63] H. Susi, D.M. Byler, J.M. Purcell, Estimation of beta structure content of proteins by means of deconvolved FTIR spectra, J. Biochem. Biophys. Methods 11 (1985) 235–240.
[64] A. Natalello, D. Ami, S. Brocca, M. Lotti, S.M. Doglia, Secondary structure, conformational stability and glycosylation of a recombinant Candida rugosa lipase studied by Fourier-transform infrared spectroscopy, Biochem. J. 385 (2005) 511–517.
[65] Y.S. Ziegler, J.J. Moresco, P.G. Tu, J.R. Yates III, A.M. Nardulli, Plasma membrane proteomics of human breast cancer cell lines identifies potential targets for breast cancer diagnosis and treatment, PLoS One 9 (7) (2014) e102341.
[66] Y.S. Ziegler, J.J. Moresco, P.G. Tu, J.R. Yates, A.M. Nardulli, Proteomic analysis identifies highly expressed plasma membrane proteins for detection and therapeutic targeting of specific breast cancer subtypes, Clin. Proteomics 15 (1) (2018) 30.
[67] D. Naumann, Infrared spectroscopy in microbiology, Enc. Anal. Chem. 102 (2000).
[68] D. Huster, A. Vogel, C. Katzka, H.A. Scheidt, H. Binder, S. Dante, T. Gutberlet, O. Zschörnig, H. Waldmann, K. Arnold, Membrane insertion of a lipidated ras peptide studied by FTIR, solid-state NMR, and neutron diffraction spectroscopy, J. Am. Chem. Soc. 125 (14) (2003) 4070–4079.
[69] A.H. Colagar, M.J. Chaichi, T. Khadjvand, Fourier transform infrared microspectroscopy as a diagnostic tool for distinguishing between normal and malignant human gastric tissue, J. Biosci. 36 (4) (2011) 669–677.